Ore Geology Reviews 90 (2017) 958–969

Contents lists available at ScienceDirect

Ore Geology Reviews

journal homepage: www.elsevier.com/locate/oregeo

# Concentrations and isotopic variability of mercury in sulfide minerals from the Jinding Zn-Pb deposit, Southwest China

Yongyong Tang [a,b], Xianwu Bi [a,*], Runsheng Yin [a,c], Xinbin Feng [d], Ruizhong Hu [a]

[a] State Key Laboratory of Ore Deposit Geochemistry, Institute of Geochemistry, Chinese Academy of Sciences, 99 Linchengxi Road, Guiyang 550081, China
[b] Department of Geological Sciences, University of Manitoba, 125 Dysart Road, Winnipeg, MB R3T2N2, Canada
[c] Environmental Chemistry and Technology Program, University of Wisconsin-Madison, 1415 Engineering Drive, Madison, WI 53706, USA
[d] State Key Laboratory of Environmental Geochemistry, Institute of Geochemistry, Chinese Academy of Sciences, 99 Linchengxi Road, Guiyang 550081, China

ARTICLE INFO

*Article history:*
Received 20 May 2016
Received in revised form 3 December 2016
Accepted 8 December 2016
Available online 9 January 2017

*Keywords:*
Mercury isotopes
Isotope fractionation
Sulfide
Jinding
Deposit

ABSTRACT

Mercury (Hg) isotopes have been proven as a useful tracer in understanding sources and biogeochemical processes of Hg in the environment. However, the use of this tracer has not yet been explored in economic geology. This paper investigates the concentrations and isotopic compositions of Hg in sulfide minerals from the Jinding deposit, the largest Zn-Pb deposit in China. Total mercury concentration (HgT) is highly variable: with the highest in sphalerite (472–1010 ng·g$^{-1}$), intermediate concentrations in pyrite (195–342 ng·g$^{-1}$) and the lowest in galena (65–310 ng·g$^{-1}$). The variation was likely due to the fact that $Hg^{2+}$ can more readily substitute for $Zn^{2+}$ than for $Fe^{2+}$ and $Pb^{2+}$, but an influence of different parental fluids on the isotopic composition of the sulfide minerals cannot be excluded. An overall range of $\delta^{202}$Hg from −3.17 to −0.57‰ is observed in the sulfides. Samples from the early stage feature the enrichments of light Hg isotopes, with $\delta^{202}$Hg ranging from −3.17 to −1.59‰, suggesting significant mass-dependent fractionation during the transport and/or deposition of Hg. However, the volatilization of aqueous Hg(0) during boiling of hydrothermal fluids was likely the most important process causing the observed fractionation. Relatively higher $\delta^{202}$Hg values (−1.84 to −0.57‰) of the late stage samples indicate that the Hg was rarely fractionated from its sources. Additionally, small but significant mass-independent fractionations are measured for the deposit with $\Delta^{199}$Hg ranging from −0.06 to 0.10‰, indicating that the Hg may have been derived from the sedimentary rocks of the Lanping Basin. Finally, we conclude that Hg isotopes have the potential to be a new tracer of sources of ore-forming materials, as well as pathways of fluid evolution in hydrothermal deposits.



## 1. Introduction

Mercury (Hg) is a redox-sensitive metal that occurs in multiple physical states on Earth. It has seven natural isotopes: $^{196}$Hg, $^{198}$Hg, $^{199}$Hg, $^{200}$Hg, $^{201}$Hg, $^{202}$Hg and $^{204}$Hg. Recent studies have revealed that Hg isotopes can undergo both mass-dependent (MDF, represented as $\delta^{202}$Hg) and mass-independent fractionation (MIF, represented as $\Delta^{199}$Hg) during a variety of physical, chemical and biological processes. For instance, Hg-MDF occurs during volatilization, adsorption, diffusion, microbial-mediated reactions and abiotic chemical reactions, which can improve our understanding of transport, transformation and bioaccumulation of Hg in surface environments (Bessinger, 2014; Blum et al., 2014; Hintelmann, 2012; Sonke and Blum, 2013; Yin et al., 2014). Additionally, Hg-MIF signatures provide unique fingerprints of some specific geochemical pathways, such as photochemical reduction (Bergquist and Blum, 2007; Zheng and Hintelmann, 2009), elemental Hg(0) volatilization (Estrade et al., 2009; Ghosh et al., 2013) and dark Hg(II) reduction (Zheng and Hintelmann, 2010). A range of >10‰ in $\delta^{202}$Hg and $\Delta^{199}$Hg to date has been reported for different geochemical reservoirs on Earth (Fig. 1). These studies demonstrate the possibility to use Hg isotopes to distinguish sources and pathways of Hg during its biogeochemical cycling.

Due to the fact that Hg is a globally distributed toxic pollutant, most Hg related studies have mainly focused on its environmental, ecological and health effects (e.g., Blum et al., 2014; Feng et al., 2004; Fitzgerald et al., 2005; Foucher and Hintelmann, 2006; Zambardi et al., 2009), whereas very few studies focused on hydrothermal deposits. Thus, the application of Hg isotopes in the field of economic geology is particularly limited. As a chalcophile element, Hg is usually found in hydrothermal sulfide minerals such as cinnabar (HgS) and sphalerite (ZnS) (Stetson et al.,

* Corresponding author.
*E-mail address:* bixianwu@vip.gyig.ac.cn (X. Bi).

http://dx.doi.org/10.1016/j.oregeorev.2016.12.009
0169-1368/

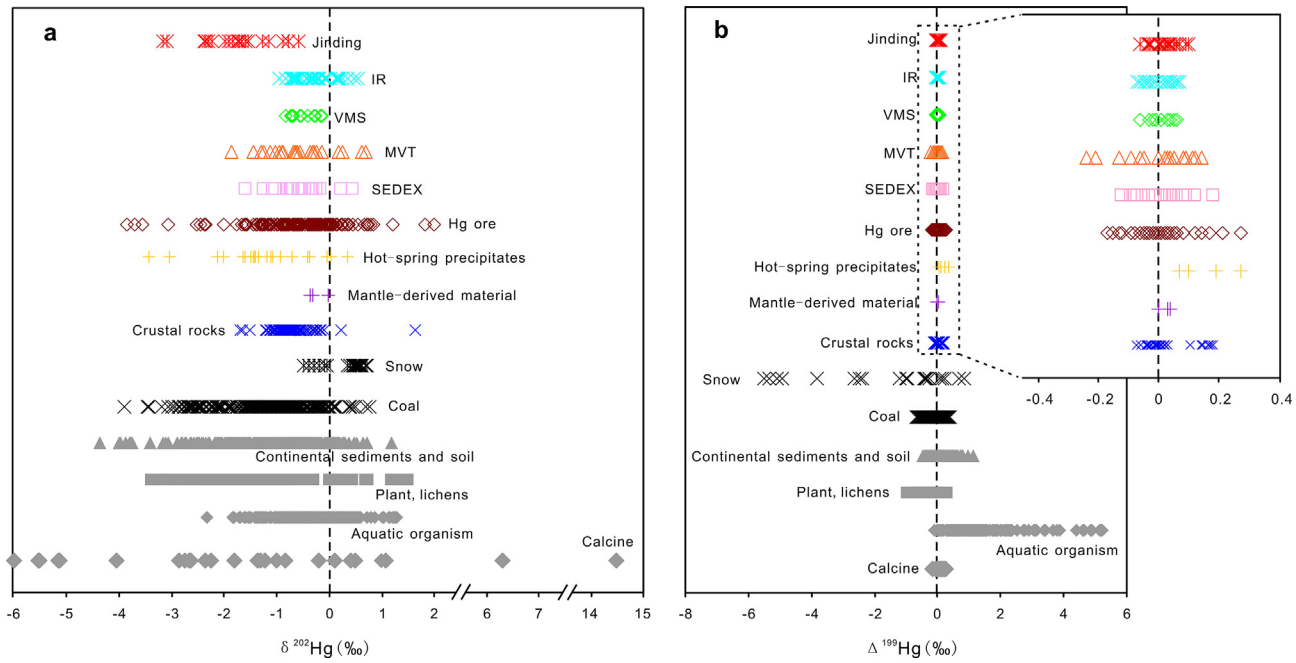


**Fig. 1.** Variations of Hg isotopes (a: $\delta^{202}$Hg; b: $\Delta^{199}$Hg) of terrestrial materials measured to date. Calcine data are from Smith et al. (2014). Aquatic organism data are from Bergquist and Blum (2007), Gantner et al. (2009), Gehrke et al. (2011), Laffont et al. (2009) and Senn et al. (2010). Plant and lichen data are from Blum et al. (2012), Carignan et al. (2009), Estrade et al. (2010) and Yin et al. (2013). Contimental sediments and soil data are from Biswas et al. (2008), Chen et al. (2012), Donovan et al. (2013), Estrade et al. (2010), Gantner et al. (2009), Gehrke et al. (2009; 2011), Gratz et al. (2010), Sherman et al. (2012), Sonke et al. (2010), Yin et al. (2013), Zambardi et al. (2009) and Zhang et al. (2013). Coal data are from Biswas et al. (2008), Lefticariu et al. (2011), Sun et al. (2014) and Yin et al. (2014). Snow data are from Sherman et al. (2010; 2012). Crustal rock data are from Blum et al. (2014) and Smith et al. (2008). Mantle-derived material data are from Sherman et al. (2009). Hot-spring precipitate data are from Sherman et al. (2009) and Smith et al. (2008). Hg ore data are from Cooke et al. (2013), Smith et al. (2005; 2008), Stetson et al. (2009), Wiederhold et al. (2013) and Yin et al. (2013). SEDEX (Sedimentary exhalative Zn-Pb deposits), MVT (Mississippi Valley-type Zn-Pb deposits), VMS (Volcanic-hosted massive sulfide deposits) and IR (Igneous-related Zn-Pb deposits) data are from Yin et al. (2016a). Data of the Jinding deposit are from this study.

2009; Yin et al., 2012). Mercury is highly volatile during the boiling of hydrothermal fluids (Smith et al., 2008; Smith et al., 2005), which may allow it to penetrate through overlying strata and form halos of Hg at surface. Mercury halos at the Earth's surface are a useful indicator in prospecting for geothermal energy and sulfide ore deposits (Bingqiu et al., 1986; Fedikow and Amor, 1990; Holland, 1972; Nelson, 1990; You and Li, 1990). In addition, Hg is generally abundant in Zn hydrothermal deposits, and smelting of Zn minerals (e.g., sphalerite) is one of the biggest anthropogenic Hg emission sources to the atmosphere (Pirrone et al., 2010). Some studies consider that Hg may be an indicator for the genesis of Pb-Zn deposits, based on the fact that Hg concentration in sphalerite is highly variable and is dependent on the genetic types of the deposits (Schwartz, 1997; Yin et al., 2012).

Currently, Hg isotopic compositions of the Earth's mantle and crust are still poorly constrained, except for a few studies that made investigations on a limited amount of lithological samples (Blum et al., 2014; Sherman et al., 2009; Smith et al., 2008). For instance, Smith et al. (2008) measured Hg contents and isotopic ratios ($\delta^{202}$Hg) of crustal rocks (including sedimentary, igneous and metamorphic) from the California Coast Range (USA), which vary from 17 to 288 ppb and −1.70 to 1.61‰, respectively. However, this level of Hg content is conspicuously higher than a recently proposed Hg abundance (mean 2.9 ± 2.6 ppb) for the Bonanza arc crust (Canil et al., 2015), likely reflecting the heterogeneity of Hg distribution in the crust. There is no data available for Hg isotopes of the mantle, other than Sherman et al. (2009) who measured the $\delta^{202}$Hg variation (−0.37 to −0.01‰) of chimney precipitates from the Guaymas Basin (USA), and hypothesized that it could represent the mantle isotopic signature. Apart from influences from source rocks, Hg isotopic compositions in sulfides may be significantly altered by isotope fractionation during transport (e.g., redox reaction, Bergquist and Blum, 2007; Zheng and Hintelmann, 2010; and boiling process, Estrade et al., 2009; Smith et al., 2008; Smith et al., 2005) and precipitation of Hg-bearing mineral phases in hydrothermal systems (Smith et al., 2015). Little or no isotopic fractionation (<±0.5‰) has been suggested to occur during release of Hg from source rocks to hydrothermal solutions, whereas boiling of hydrothermal fluids can cause large isotopic fractionation (>5‰) during the migration from source rocks to the deposition sites (Smith et al., 2008; Smith et al., 2005). Yin et al. (2016a) recently reported marked Hg-MIF ($\Delta^{199}$Hg: −0.24 to 0.18‰, n = 102) in addition to MDF ($\delta^{202}$Hg: −1.87 to 0.70‰, n = 102) among genetically diverse Zn deposits in China, shedding light on the potential of Hg isotopes to identify sources of Hg. However, such an application has not been tested in any specific deposits.

The Jinding deposit in western Yunnan Province, China, is the largest Zn mineral deposit in Asia and contains metal reserves of >15 Mt (Xue et al., 2007a). Although the origin of the deposit has long been in dispute (e.g., Bai et al., 1985; Gao et al., 2005; Hou et al., 2008; Hu et al., 1998; Leach et al., 2016; Shi et al., 1983; Wang and Li, 1991; Xue et al., 2007a; and references therein), there is a growing consensus that the deposit was formed from basinal brine-dominated fluids with ore-forming materials largely derived from crustal sources (e.g., Hu et al., 1998; Hu et al., 2013; Li, 1998; Kyle and Li, 2002; Song et al., 2011; Tang et al., 2014). Since the deposit has been extensively studied with a huge accumulation of geological and geochemical data, it creates a good opportunity to explore the application of Hg isotopes to economic geology. This paper investigates the concentrations and isotopic compositions of Hg in different stage sulfides (pyrite, sphalerite and galena) from the Jinding Zn-Pb deposit with two main objectives: 1) to determine the variability of Hg concentrations and isotopes in the

deposit and discuss the possible causes of variability; and 2) to discuss the indicative significance of Hg isotopes to the genesis of the deposit and demonstrate the feasibility of using Hg isotopes as a new tracer in economic deposits.

## 2. Backgrounds

### 2.1. Regional geology

The Jinding deposit is located in the north-central part of the Lanping Basin, which is an intra-continental basin developed on the Changdu-Lanping-Simao microplate (Fig. 2). The Changdu-Lanping-Simao microplate was initially formed when the Proto-Tethys Ocean was closed near the end of the Silurian (Xue et al., 2007a). As the Paleo-Tethys Ocean opened in the Late Paleozoic, the microplate was split off by the Paleo-Jinshajiang Ocean from the Yangtze Plate on the east, and the Paleo-Lancangjiang Ocean from the Tibet-Yunnan Plate on the west (Liu et al., 1993). The oceanic slabs subducted beneath the microplate in the Late Permian, and resulted in the development of volcanic islands along both edges of the microplate (Mo et al., 1993). The Paleo-Tethys Ocean was closed because of an arc-continental collision in the Early Triassic (Li et al., 1999). Post-collision extension in the Middle to Late Triassic led to the Changdu-Lanping-Simao block rifting to form the Lanping rift basin. Consequent bimodal volcanic rocks occur in the east and west of the Lanping Basin, whereas shallow marine clastics, carbonates and sandy mudstone sequences filled the basin (Pan et al., 2003; Zhong et al., 2006). Following the closure of the Bangong-Nujiang Ocean in the Jurassic, the rift basin transitioned to a sag basin (Liu et al., 1993; Spurlin et al., 2005; Yin and Harrison, 2000). The basin is filled by Jurassic and Cretaceous rocks which are largely marine-terrestrial red-beds and minor carbonates (Mu et al., 1999). Continuous contraction associated with the Cenozoic India-Asia continent collision resulted in the formation of a series of discrete Tertiary foreland basins over the Mesozoic sag basin at the eastern margin of the Tibetan Plateau (Li et al., 2006; Spurlin et al., 2005; Wang and Burchfiel, 1997). The Lanping Basin is one of these Tertiary foreland basins. The Himalayan orogeny strongly folded and faulted the basin strata, and they were intruded by Cenozoic igneous intrusions (Xue et al., 2003).

### 2.2. Deposit geology

The Jinding deposit extends over approximately 8 km$^2$ and consists of 7 mining sections, namely, the Beichang, Paomaping, Jiayashan, Fengzishan, Nanchang, Xipo and Baicaoping sections (Fig. 3). The rocks in the mining area are divided by a thrust fault ($F_2$) into the upper allochthonous overturned sequence and the lower autochthonous normal sequence. The allochthon consists of, from top to bottom, the Upper Triassic Waigucun Formation purple thick-bedded mudstones and siltstones, Sanhedong Formation bitumen-containing limestones, Maichuqing Formation gray carbonaceous plant debris-bearing silty mudstones interlaid with fine sandstone pods, the Middle Jurassic Huakaizuo Formation purple muddy siltstones, and the Lower Cretaceous Jingxing Formation light gray sandstones. The autochthon is made up of the Paleocene Yunlong Formation brick-red conglomerates and gravelly sandstones, passing westward through sandstones to evaporitic mudstones, the Upper Cretaceous Hutousi Formation light gray to purplish fine-grained quartz sandstone and the Nanxin Formation rhythmically interbedded conglomerates, sandstones and siltstones.

Orebodies mainly occur in the Jingxing and Yunlong Formations, the hanging- and foot-wall of $F_2$, respectively. The country rocks are hydrothermally altered with pyrite, calcite, silica, celestine, gypsum and hematite. The deposit experienced a complex history, generally beginning from sedimentary diagenesis through hydrothermal mineralization followed by supergene activity, wherein the hydrothermal process can be divided into early and late stages according to distinct mineral textures (Figs. 4 and 5). The early-stage mineralization is characterized by fine-grained sulfides disseminated in sandstones (Fig. 4a) or conglomerates (carbonate breccia), which is dominant in the deposit. The typical association includes sphalerite, pyrite and a minor proportion of galena, along with quartz and calcite. The sulfides usually occur as cements interstitial to clasts in sandstones after replacement of sedimentary carbonate matrix (Fig. 4c), or fill in spaces among carbonate breccias. In contrast, the late-stage mineralization is mainly represented by cross-cutting veins of coarse-grained galena (Fig. 4b and d), accompanied by sphalerite and pyrite. Additionally, coarse-grained celestine and calcite are often present along with galena, occurring in fractures or cavities in carbonate breccias and gravelly sandstones.

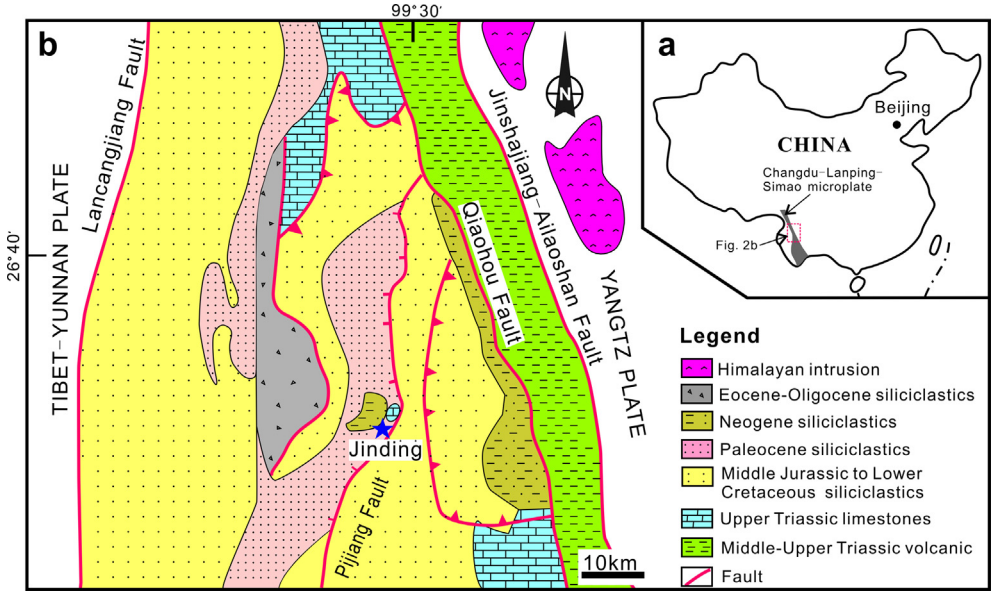


**Fig. 2.** Geological map of the Lanping Basin showing the location of the Jinding deposit (after Kyle and Li, 2002).

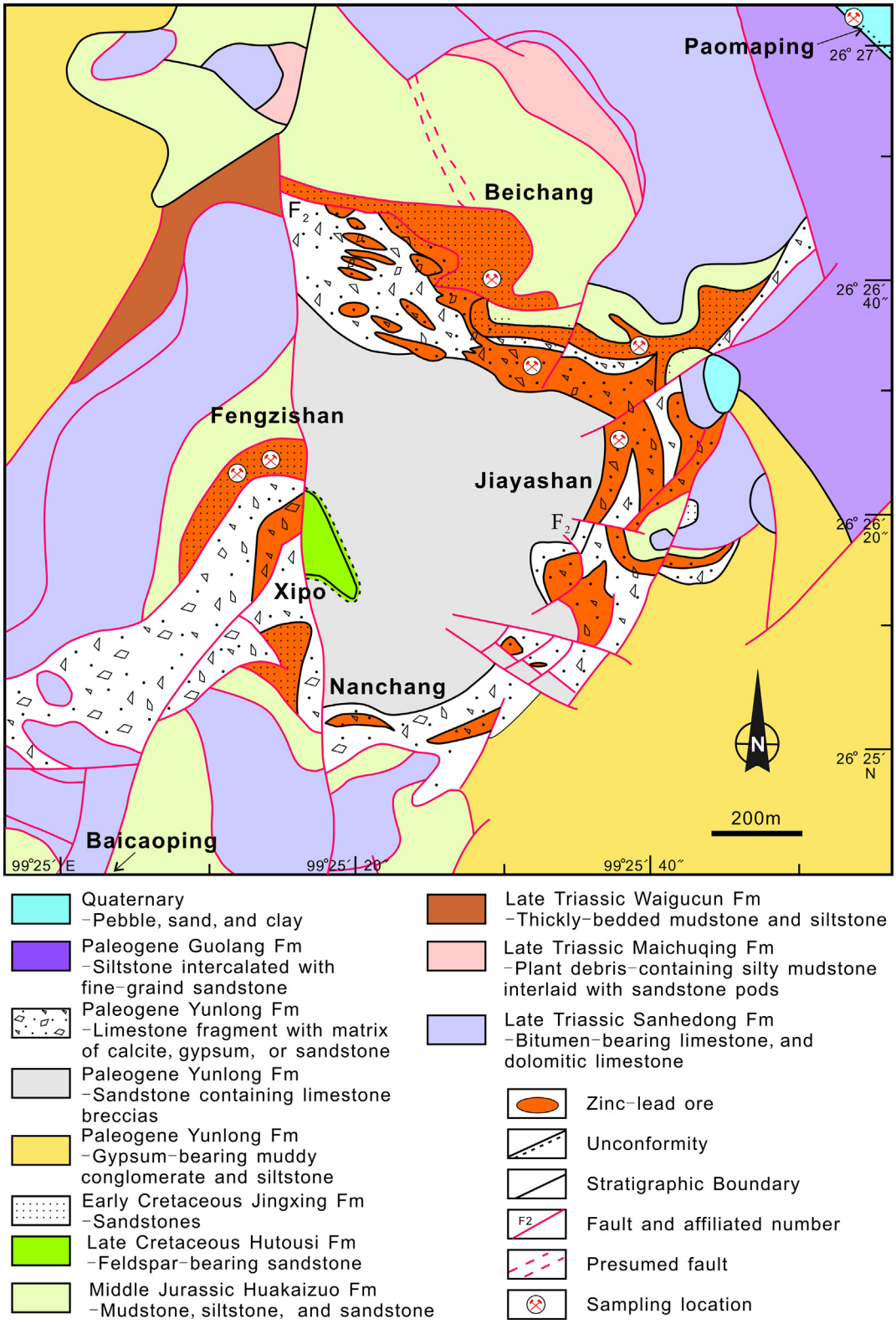


**Fig. 3.** Geological map of the Jinding Zn-Pb deposit, showing main stratigraphic units, faults and sampling locations (after Third Geological Team, 1984).

## 3. Sample preparations and experimental procedures

Samples were collected from varying elevations of the mining sections in Beichang, Paomaping and Jiayashan with descriptions shown in Table 1. According to the occurrences indicative of mineral generations, fine crystal samples of early stage were usually crushed to within 40–80 μm for magnetic selection followed by handpicking under a binocular microscope; late stage galena were separated by handpicking after being crushed (<250 μm). Afterwards, the selected mono-mineral samples were ground into powder in an agate mortar for Hg concentration and isotope analysis.

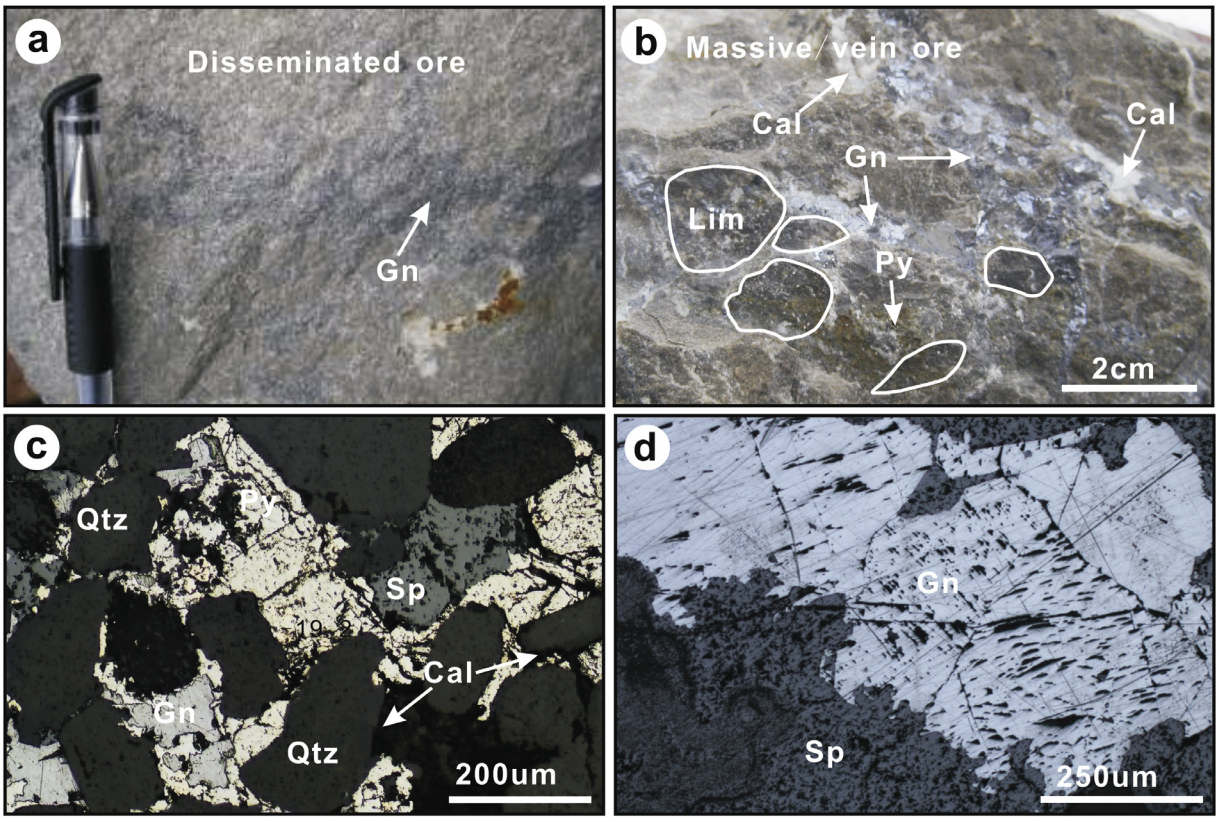


**Fig. 4.** Photographs of ore textures and mineralogy from the Jinding deposit. a. Early-stage disseminated sulfides are cut by a late stage galena vein. b. Massive/vein ore shows a late-stage coarse-grained galena vein crosscutting early-stage pyrite cements interstitial to limestone breccias. c. Early-stage disseminated sulfide grains cementing siliciclastics in sandstones. d. Late-stage coarse-grained galena vein crosscutting early-stage sphalerite. Mineral abbreviations: Cal-calcite, Gn-galena, Lim-limestone breccia, Py-pyrite, Qtz-quartz, Sp-sphalerite.

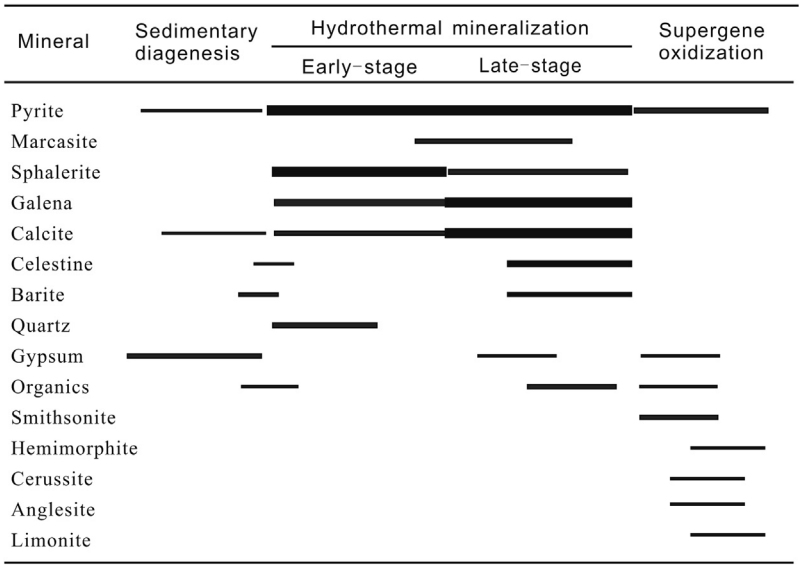


**Fig. 5.** Simplified paragenetic sequence of major sulfides and gangue minerals from the Jinding deposit (modified after Zhao, 2006).

Approximately 0.2 g of each sample was digested using 5 mL aqua regia (HCl: $HNO_3$ = 3:1) at 95 °C for 30 min. The digest solution was diluted to 25 mL prior to analysis by cold vapor atomic absorption spectrometry (CVAAS, F732-S, Shanghai Huaguang Instrument Co., Ltd.) at the Institute of Geochemistry (Chinese Academy of Sciences), with a detection limit of 0.1 ng·mL$^{-1}$ (Li et al., 2005). Certified reference material GBW07168 (Zn concentrate) was prepared to ensure the accuracy of HgT measurements. The measured HgT for GBW07168 was 560 ± 80 ug·g$^{-1}$ (n = 5), in agreement with the certified value of 547 ± 92 ug·g$^{-1}$ (Yin et al., 2012). Coefficients of variation from duplicate digests of each sample were <11%. Based on the measured HgT concentrations, sample solutions were diluted to 2 ng·mL$^{-1}$ prior to Hg isotope analysis by a Neptune Plus multi-collector inductively coupled plasma mass

**Table 1**
Sample description and data summary used in this study.

| Sample | Mineral | Types of Mineralization | Location | Stage | Elevation (m) | HgT ($ng \cdot g^{-1}$) | $\delta^{202}Hg$ (‰) | 2σ (‰) | $\Delta^{199}Hg$ (‰) | 2σ (‰) | $\Delta^{200}Hg$ (‰) | 2σ (‰) | $\Delta^{201}Hg$ (‰) | 2σ (‰) | $\delta^{34}S$ (‰) |
|---|---|---|---|---|---|---|---|---|---|---|---|---|---|---|---|
| JD09-12 | Py | Disseminated | B | Early | 2688 | 251 | −2.29 | 0.06 | 0.04 | 0.02 | −0.07 | 0.03 | 0.05 | 0.02 | 20.7 |
| JD09-55 | Py | Massive | B | Early | 2742 | 342 | −3.17 | 0.09 | 0.05 | 0.02 | −0.02 | 0.01 | 0.01 | 0.01 | 16.2 |
| JD09-23 | Py | Massive | P | Early | 2735 | 228 | −3.09 | 0.05 | 0.06 | 0.04 | 0.06 | 0.01 | 0.04 | 0.02 | 20.6 |
| JDJ10-13 | Py | Disseminated | J | Early | 2732 | 195 | −2.36 | 0.07 | 0.03 | 0.01 | 0.00 | 0.04 | 0.09 | 0.00 | 25.5 |
| JD-05 | Sp | Disseminated | B | Early | 2679 | 1010 | −1.60 | 0.03 | −0.02 | 0.09 | 0.01 | 0.01 | −0.01 | 0.03 | 17.1 |
| JD11-19 | Sp | Disseminated | B | Early | 2736 | 898 | −1.91 | 0.08 | 0.07 | 0.01 | −0.01 | 0.04 | −0.04 | 0.03 | 12.0 |
| JD-44 | Sp | Massive | B | Early | 2667 | 540 | −1.66 | 0.06 | −0.04 | 0.03 | 0.02 | 0.01 | −0.04 | 0.02 | N.D. |
| JD-49 | Sp | Massive | B | Early | 2663 | 790 | −1.74 | 0.10 | 0.01 | 0.02 | 0.03 | 0.00 | 0.02 | 0.04 | N.D. |
| JD-59 | Sp | Massive | B | Early | 2698 | 640 | −1.59 | 0.11 | −0.06 | 0.01 | 0.02 | 0.01 | −0.02 | 0.00 | 15.0 |
| JD11-46b | Sp | Disseminated | J | Early | 2732 | 929 | −2.23 | 0.09 | 0.03 | 0.02 | 0.04 | 0.01 | 0.05 | 0.02 | N.D. |
| JD10-17A | Sp | Disseminated | J | Early | 2720 | 598 | −1.99 | 0.02 | 0.02 | 0.05 | 0.03 | 0.03 | 0.01 | 0.03 | 20.9 |
| JDPMP2 | Sp | Disseminated | P | Early | 2700 | 472 | −2.38 | 0.02 | 0.09 | 0.03 | −0.01 | 0.01 | −0.06 | 0.05 | 16.4 |
| JD-21 | Sp | Massive | P | Early | 2735 | 570 | −1.72 | 0.03 | −0.04 | 0.05 | 0.02 | 0.01 | −0.02 | 0.01 | 16.5 |
| JD09-55 | Ga | Vein | B | Late | 2742 | 65 | −1.14 | 0.07 | 0.05 | 0.00 | 0.02 | 0.03 | −0.02 | 0.00 | N.D. |
| JDPMP6 | Ga | Vein | P | Late | 2700 | 152 | −1.55 | 0.02 | 0.07 | 0.04 | −0.01 | 0.01 | 0.04 | 0.01 | N.D. |
| JD09-10 | Ga | Massive | B | Late | 2672 | 173 | −1.26 | 0.08 | 0.10 | 0.02 | 0.03 | 0.03 | 0.12 | 0.02 | N.D. |
| JD-44 | Ga | Massive | B | Late | 2667 | 310 | −0.78 | 0.03 | 0.00 | 0.05 | −0.02 | 0.00 | −0.04 | 0.03 | 12.1 |
| JD-49 | Ga | Vein | B | Late | 2663 | 130 | −0.78 | 0.05 | −0.03 | 0.06 | 0.00 | 0.02 | −0.02 | 0.01 | −6.0 |
| JD-59 | Ga | Massive | B | Late | 2698 | 150 | −0.79 | 0.00 | −0.03 | 0.04 | −0.03 | 0.07 | −0.02 | 0.00 | N.D. |
| JDBC1 | Ga | Vein | B | Late | 2665 | 160 | −1.84 | 0.09 | 0.01 | 0.01 | 0.03 | 0.03 | −0.02 | 0.02 | −5.8 |
| JD-21 | Ga | Vein | B | Late | 2735 | 210 | −0.87 | 0.09 | 0.03 | 0.00 | 0.03 | 0.00 | −0.02 | 0.03 | 12.6 |
| JD-05 | Ga | Vein | B | Late | 2679 | 230 | −0.57 | 0.04 | 0.03 | 0.00 | 0.02 | 0.01 | 0.03 | 0.03 | N.D. |

Note: $\delta^{34}S$ was measured using the Continuous Flow Mass Spectrometry at the State Key Laboratory of Environmental Geochemistry, Institute of Geochemistry, Chinese Academy of Sciences, with the analytical accuracy of ±0.1‰ (2σ). Mineral abbreviation: Ga-galena, Py-pyrite, Sp-sphalerite. Location: B-Beichang, J-Jiayashan, P-Paomaping. N.D. means not determined.

spectrometry (MC-ICP-MS) housed at the University of Wisconsin-Madison (USA). The instrument was connected with a gas-liquid phase separator and an Apex-Q desolvation unit (Elemental Scientific Inc., USA) for Hg and Tl introduction, respectively. Stannous chloride ($SnCl_2$ 3% in 10% HCl, w/v) and Hg solutions were continuously pumped onto a frosted glass phase separator, producing gaseous elemental Hg(0) which was mixed with dry Tl aerosol generated by the Apex-Q nebulizer, before being introduced into the MC-ICP-MS. The Apex-Q was set in the free flow-mode using the "sample" gas of the MC-ICP-MS, and the gas-liquid phase separator was flushed by the "additional" gas of the instrument. The standard material Tl (NIST SRM 997, $^{205}Tl/^{203}Tl = 2.38714$) was used as an internal standard for simultaneous instrumental mass bias correction for Hg (Yin et al., 2016b). Seven of nine faraday cups: L3, L2, L1, C, H1, H2 and H3, were used to monitor the $^{198}Hg$, $^{199}Hg$, $^{200}Hg$, $^{201}Hg$, $^{202}Hg$, $^{203}Tl$ and $^{205}Tl$ isotopes, respectively. A nickel and X skimmer cone combined with a jet cone were used. The gains of the amplifier associated with each faraday cup were calibrated for efficiency on a daily basis. Instrument parameters (e.g., Ar gas flow, torch settings, and lens system) were tuned for a maximum ion intensity of Hg and Tl in standard solutions. The concentration of the Hg and acid in NIST SRM 3133 was diluted to be within 10% of the sample digests. HgT in the sample digest was also measured by the MC-ICP-MS using $^{202}Hg$ signals. HgT concentrations measured by MC-ICP-MS were 91 to 109% of that measured by CVAAS.

Following the convention recommended by Blum and Bergquist (2007), Hg-MDF is expressed in $\delta^{xxx}Hg$ notation referenced to the NIST-3133 Hg standard (analyzed before and after each sample):

$$\delta^{xxx}Hg(‰) = [(^{xxx}Hg/^{198}Hg_{sample})/(^{xxx}Hg/^{198}Hg_{standard}) - 1] \times 1000 \quad (1)$$

Hg-MIF is reported in Δ notation ($\Delta^{xxx}Hg$) and it describes the deviation from mass dependence (2):

$$\Delta^{xxx}Hg \approx \delta^{xxx}Hg - \delta^{202}Hg * \beta \quad (2)$$

where β is the isotope-specific scaling factor determined by the laws of MDF, which is equal to 0.2520 for $^{199}Hg$, 0.5024 for $^{200}Hg$, and 0.7520 for $^{201}Hg$ (Blum and Bergquist, 2007). The UM-Almadén standard solution (0.5 to 2.0 $ng \cdot mL^{-1}$) with acid concentration matched with the NIST 3133 was measured every 10 samples. The reproducibility of Hg isotope data was assessed by measuring two duplicate digests of each sample. Data uncertainties adopted the larger value of either the external precision of the replicate standard solutions or the measurement uncertainty of duplicate sample digests. The overall average and uncertainty of UM-Almadén ($\delta^{202}Hg$: −0.48 ± 0.08‰; $\Delta^{199}Hg$: −0.02 ± 0.03‰; $\Delta^{200}Hg$: +0.01 ± 0.03‰; $\Delta^{201}Hg$: −0.03 ± 0.03‰, 2σ, n = 9) agreed well with previous studies (e.g., Blum and Bergquist, 2007).

## 4. Results

Concentrations and isotopic compositions of Hg in sulfide minerals are shown in Table 1. Total mercury content (HgT) varies greatly among sulfide species (Fig. 6a): the highest values are observed in sphalerite (472–1010 $ng \cdot g^{-1}$, mean 716 $ng \cdot g^{-1}$), intermediate values in pyrite (195–342 $ng \cdot g^{-1}$, mean 254 $ng \cdot g^{-1}$) and the lowest in galena (65–310 $ng \cdot g^{-1}$, mean 176 $ng \cdot g^{-1}$). Mercury is largely hosted in the early stage sulfides where sphalerite is quantitatively dominant.

The sulfides show a wide variation in Hg isotopes ($\delta^{202}Hg$: −3.17 to −0.57‰; Fig. 6b). Early stage mineralization is characterized by enrichments of light Hg isotopes, wherein the pyrite exhibits the lowest $\delta^{202}Hg$ values, ranging from −3.17 to −2.29‰ with a mean of −2.73‰, and the sphalerite follows (−2.38 to −1.59‰, mean −1.87‰). Late stage mineralization, represented by coarse-grained galena, shows relative enrichments of heavy isotopes, and their $\delta^{202}Hg$ values vary from −1.84 to −0.57‰ with a mean of −1.06‰.

There is no correlation between the elevation of sampling and HgT of the sulfides (Fig. 7a). Over 80% of analyzes of $\delta^{202}Hg$ for the early stage sulfides are linearly dependent on the elevations of sampling with $R^2$ of 0.5883, where higher elevations tend to be more enriched in light Hg isotopes (Fig. 7b). The Hg isotope ratios of late stage galena samples show little correlation to the sampling elevation, in contrast to that of the early stage sulfides. The Jinding sulfides have slight Hg-MIF, with $\Delta^{199}Hg$ that range

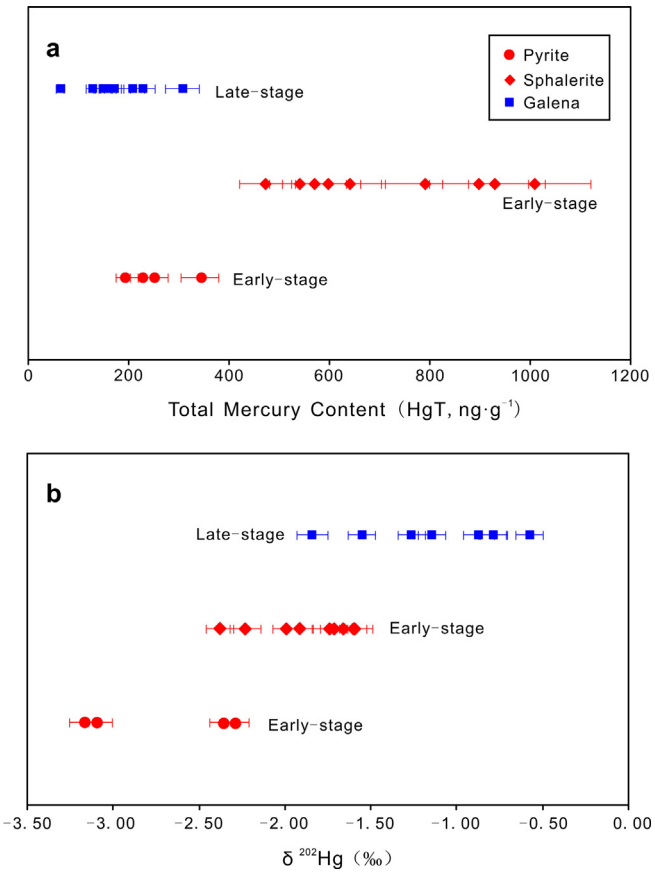


**Fig. 6.** Variations of HgT (a) and $\delta^{202}$Hg (b) in the early and late stage sulfides. The error bars of HgT indicate 11% of Hg contents, and those of $\delta^{202}$Hg represent the 2σ uncertainties.

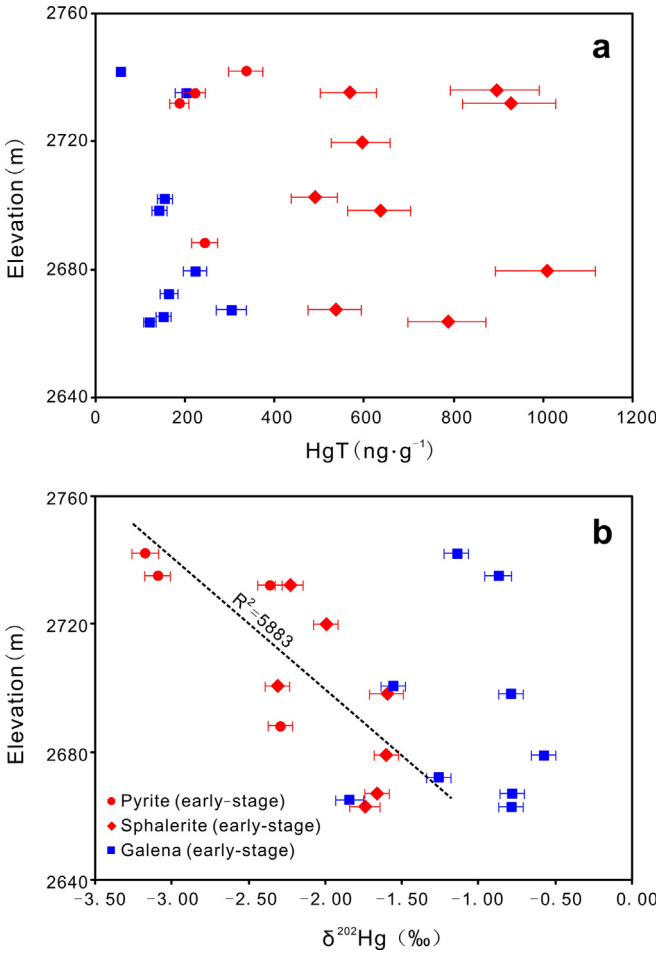


**Fig. 7.** Covariation of the sampling elevations vs. HgT (a) and $\delta^{202}$Hg (b) in the Jinding deposit. a. No clear relationship is shown between sampling elevations and HgT values. b. The $\delta^{202}$Hg values of early stage pyrite and sphalerite (except the samples of JD11-19 and JD-21) appear to decrease with increasing sampling elevations, whereas the late stage $\delta^{202}$Hg are less correlated with sampling elevations. The elevation is above sea level.

from −0.06 to 0.10‰. The sulfide $\Delta^{199}$Hg values are indistinguishable between stages, and no correlations are observed with either $\delta^{202}$Hg or HgT.

## 5. Discussion

### 5.1. Factors affecting the HgT in sulfides

Although Hg-rich minerals, such as cinnabar, metacinnabar, montroydite (HgO), tiemannite (HgSe) and coloradoite (HgTe), are usually absent from Pb-Zn deposits, individual deposits have been reported to contain a few occurrences of inclusions that give rise to high contents of Hg in sulfides (e.g., Grammatikopoulos et al., 2006; Saulas, 1985; Schwartz, 1997; Yin et al., 2012). For instance, sphalerite from the Eskay Creek deposit (British Columbia, Canada) have Hg concentration as high as 16 wt% because of included Hg-tetrahedrite and cinnabar (Grammatikopoulos et al., 2006). Previous studies suggest that Zn deposits with cinnabar could be regarded as an unusual type of mineralization, transitional between mercury and zinc deposits (Schwartz, 1997). However, there is no evidence that any Hg-rich minerals are present in the Jinding deposit. Sphalerite is the most major carrier of Hg in the deposit, with HgT values ranging from 472 to 1010 ng·g$^{-1}$ (mean 716 ng·g$^{-1}$), much lower than that of SEDEX (mean 48 μg·g$^{-1}$) or MVT deposits (mean 10 μg·g$^{-1}$; Yin et al., 2012). This not only confirms the scarcity of Hg-rich minerals, but may also suggest a difference in origin of the Jinding deposit from MVT and SEDEX deposits. Additionally, analytical surface scans over polished ore sections do not show any sign of microscale inclusions rich in Hg. Although it is not sufficient enough to completely exclude the presence of small Hg-mineral inclusions, their influence is considered to be limited or insignificant to Hg concentrations of sulfides in the deposit.

Thus, isomorphic substitution of Hg is invoked, which involves the substitutions for Zn, Fe and Pb in sphalerite, pyrite and galena, respectively. The substitution of minor and trace elements in sphalerite is largely governed by the substitution of ions for tetrahedrally-coordinated $Zn^{2+}$, which is based primarily on size and affinity for tetrahedral coordination (Cook et al., 2009). Since the radius of $Hg^{2+}$ (0.102 Å) is similar to that of $Zn^{2+}$ (0.074 Å) and common Hg-bearing mineral, e.g., metacinnabar, isostructurally belong to the sphalerite group (Liu et al., 1984; Vaughan and Rosso, 2006), this may lead $Hg^{2+}$ to more readily be incorporated into sphalerite than pyrite and galena. Thus, the HgT values of sphalerite are much higher than those of pyrite and galena. Additionally, the low contents of Hg in pyrite and galena (Fig. 6a), could also be attributed to small inclusions of sphalerite. In this case, a similar variation of Hg isotopes should have been displayed. However, this is not observed (Fig. 6b), supporting that Hg largely exists as isomorphic substitutes of $Fe^{2+}$ and $Pb^{2+}$ in pyrite and galena, respectively.

Apart from the occurrence of Hg in sulfides, the fluid properties may impose potential constraints on the HgT of sulfides. Jinding

fluid inclusions suggest that the fluid responsible for the early-stage mineralization was largely from basinal brines with high temperature and salinity (150–300 °C, >8 wt% $NaCl_{eq}$), whereas the late-stage fluid was meteoric water with low temperature and salinity (50–150 °C, <8 wt% $NaCl_{eq}$; Tang et al., 2011). The change of salinity between the early and late stage ore fluids influences the HgT in the resulting sulfides, since Hg has been proven to be preferentially carried in high salinity solutions (Fein and Williams-Jones, 1997). Lastly, the amount of organic materials dissolved in the ore fluids, which were widespread but difficult to quantify in the deposit (Xue et al., 2007b), could also impose on Hg transportation, as Hg can easily form stable complexes with a variety of organic compounds (e.g., Smith and Martell, 1989; Tissot and Welte, 1984).

### 5.2. Sulfide Hg isotopic compositions

At present, it is considered that the Jinding deposit largely derived ore-forming metals from crustal sources; for example, lead isotopic compositions suggest that the Pb was mainly derived from the upper crustal sedimentary rocks of the Lanping Basin (Tang et al., 2013; Wang et al., 2009; Xiu et al., 2006; Zhao, 2006), while Sr isotopes are evidence for a mixture of Sr from the marine carbonates and sedimentary clastic rocks (Hu et al., 2013; Li, 1998; Luo et al., 1994; Tang et al., 2013). The Hg largely occurs in association with Pb-Zn sulfides, indicating that it has the same sources as the lead and zinc. However, it is not allowed to directly constrain the Hg isotope compositions of those potential source rocks in the Lanping Basin due to the lack of relevant data for this area. Nevertheless, compared to the $\delta^{202}$Hg data of crustal rocks (mean −0.73 ± 0.44‰, 1σ, n = 69, Fig. 1a), the Jinding deposit shows a wide range of $\delta^{202}$Hg values (mean −1.70 ± 0.72‰, 1σ, n = 22) and is enriched in light isotopes, in particular, in the early stage sulfides. This indicates significant Hg-MDF during transport and/or deposition, if the variation of $\delta^{202}$Hg is assumed to remain consistent in crustal rocks elsewhere in the world.

The large variations of $\delta^{202}$Hg often observed among HgS deposits and hot-spring precipitates are suggested to result from Hg-MDF during boiling of hydrothermal fluids in the subsurface (e.g., Sherman et al., 2009; Smith et al., 2008; Smith et al., 2005). Sonke et al. (2010) invoked the boiling process to explain the variation in $\delta^{202}$Hg (−1.25 to 0.46‰) of sphalerite from the Mount Isa and Broken Hill Pb-Zn deposits. Mercury is the only metal that vaporizes during boiling in low temperature hydrothermal systems (Spycher and Reed, 1989), and the process has been experimentally proven to cause $\delta^{202}$Hg fractionation of over 1‰ (Zheng et al., 2007). Therefore, boiling is most likely a major process responsible for the variation observed in this study. In general, pore fluids or formation fluids released by sediments during burial or dehydration would be reduced, in which Hg exists dominantly as Hg(0) (Barnes and Seward, 1997). Strong tectonic movements can expel Hg-bearing fluids out of their host rocks and drive the fluids to ascend along deep-seated faults. The relief of pressure would trigger aqueous Hg-bearing fluids to boil and release vapor Hg(0), which favors lighter isotopes. A weakly negative correlation of $\delta^{202}$Hg with sampling elevations for the early stage sulfides (Fig. 7b) confirms this hypothesis, similar to that observed in the National and Ivanhole districts (Smith et al., 2005), where the Hg in the upper part of boiling fluid systems is isotopically light relative to that in the lower part. Individual outliers might reflect the interference of Hg from deep fluids or late stage hydrothermal fluids. Considering the relatively low solubility of Hg(0) in aqueous solutions, boiling is probably not the only mechanism resulting in the large variation of $\delta^{202}$Hg in the Jinding deposit. Other possibilities are, for instance, that reduction of Hg(II) by both inorganic and biological reactions to Hg(0) could cause larger fractionations in combination with volatilization of aqueous Hg(0) to gaseous Hg (0) (Bergquist and Blum, 2007; Fitzgerald and Lamborg, 2003; Zheng and Hintelmann, 2010).

Precipitation of sulfides is another process that can potentially affect the variation of Hg isotopes. Most recently, an experimental investigation was conducted on Hg isotope fractionation during precipitation of metacinnabar that reveals a fractionation of −0.63‰ between $\delta^{202}$Hg of precipitates and those of dissolved Hg associated with an equilibrium fractionation effect during the transition of O- to S-coordination of Hg(II) in solution (Smith et al., 2015). The effect of light isotope enrichments occurring in sulfide precipitates has also been observed for Fe (Butler et al., 2005), Cu (Ehrlich et al., 2004) and Zn (Veeramani et al., 2015), notwithstanding that different mechanisms are invoked to explain these fractionations. For example, the isotopic behaviors of Fe and Zn during precipitation of FeS and ZnS are attributed to kinetic effects (Butler et al., 2005; Veeramani et al., 2015), while the Cu isotopic fractionation of covellite (CuS) from aqueous Cu(II) may not be controlled by the precipitation step but the reduction of Cu(II) to Cu(I) (Ehrlich et al., 2004).

Galena samples from the late stage mineralization have higher $\delta^{202}$Hg values than the early stage pyrite and sphalerite, and they do not appear to show any trend between $\delta^{202}$Hg and sampling elevations (Fig. 7b). There is evidence that suggests different hydrothermal fluids for the mineralization of early and late stage minerals and they are distinct in terms of physico-chemical properties and isotopic compositions (Li, 1998; Luo et al., 1994; Tang et al., 2014; Wen et al., 1995; Xue et al., 2007). As stated above, relatively high temperature and saline fluids are inferred by fluid inclusion microthermometry for the early stage mineralizatation, but low temperature and saline fluids are inferred for the late stage. This is further constrained by the H–O and C–O isotope data that suggest the early stage fluids would have been derived from formational waters generated by dissolution of marine carbonates, while late stage fluids were dominated by meteoric water (Luo et al., 1994; Qin and Zhu, 1991; Tang et al., 2013; Zeng, 2007). This contrast leads us to believe that the Hg of the late stage fluids should have been derived from different sources than those of the early stage fluids, or they had experienced different degrees of isotopic fractionation during their transport.

Small but significant Hg-MIF is observed in the Jinding deposit. The overall range of 0.16‰ in $\Delta^{199}$Hg is much higher than the analytical uncertainty for UM-Almadén (0.03‰, 2σ, n = 9). Hg-MIF is mainly caused by the nuclear volume effect (NVE; Schauble, 2007) and magnetic isotope effect (MIE; Buchachenko, 2013) during various biogeochemical processes, such as, elemental Hg(0) volatilization (Estrade et al., 2009; Ghosh et al., 2013), equilibrium Hg-thiol complexation (Wiederhold et al., 2010), dark Hg(II) reduction (Zheng and Hintelmann, 2010) and photochemical reactions (Bergquist and Blum, 2007; Chandan et al., 2014; Zheng and Hintelmann, 2009, 2010). Photochemical reactions are thought to be the main processes that generate Hg-MIF observed at the Earth's surface (Bergquist and Blum, 2009; Blum et al., 2014; Sonke, 2011; Yin et al., 2014). Several samples with reliable MIF have $\Delta^{199}$Hg/$\Delta^{201}$Hg ratios of 1 ± 0.3 (σ, n = 8), approximate to the photoreductive $\Delta^{199}$Hg/$\Delta^{201}$Hg of 1–1.3 (Bergquist and Blum, 2007), which indicate that this Hg-MIF was likely induced by MIE during photochemical reduction of Hg(II) (Bergquist and Blum, 2007; Chandan et al., 2014; Wiederhold, 2015). As for the remaining samples, they show ambiguous MIF with anomalous $\Delta^{199}$Hg/$\Delta^{201}$Hg ratios, which might result from their relatively large uncertainties or indicate some other processes responsible for the MIF (e.g., Estrade et al., 2009; Zheng and Hintelmann, 2009).

Considering the recycling of the Earth's surface materials, the Hg-MIF signature formed during exposure to sunlight could be recorded in various rocks and minerals after it returns to the inte-

rior crust, and thus has the potential to trace sources of Hg in mineral deposits (Yin et al., 2016a). Natural samples show large variations of Hg-MIF, but for most lithospheric samples a small range of about 0.5‰ in $\Delta^{199}$Hg is observed (Fig. 1b). Hot-spring precipitates, MVT and SEDEX deposits have been observed with relatively significant MIF signatures, due to the fact that Hg was cycled through the atmosphere or the material sources carrying Hg were exposed to sunlight and underwent photochemical MIF (Sherman et al., 2009; Sonke et al., 2010; Yin et al., 2016a). Both stages of sulfides in the Jinding deposit have indiscriminate Hg-MIF, with $\Delta^{199}$Hg largely falling within the range of sedimentary rocks (Fig. 8). This is in agreement with the Pb isotope data, suggesting that the sedimentary rocks of the Lanping Basin are sources of the Pb, as well as Hg. The difference in $\delta^{202}$Hg between the early and late stage samples would be a result of different pathways of Hg evolving in separate fluids. The similarity of $\delta^{202}$Hg of late stage samples to those of sedimentary rocks argues that the Hg underwent little fractionation from its sources.

### 5.3. Implications for origin of the deposit

Both the early and late stage samples display a similar $\Delta^{199}$Hg variation to that of sedimentary rocks, which is likely attributed to same sources of Hg from the sedimentary rocks of the Lanping Basin. It is plausible that a sedimentary Hg-MIF signature was mobilized and transferred by hydrothermal fluids to the deposited ores. However, the discrepancy in Hg-MDF between stages implies different isotopic fractionation pathways of Hg during transport by fluids. Additionally, no obvious correlation is observed between $\delta^{34}$S and $\delta^{202}$Hg of the early and late stage sulfides (Fig. 9), which is better explained by mixing of a Hg-bearing (with Pb and Zn, as well) fluid and a sulfur-bearing fluid at the depositional site, whereas the S and Hg in the early stage fluids should have been isotopically distinct from those of late stage fluids. The $\delta^{34}$S values range from −25.5 to −12.0‰ and −12.6 to −5.8‰ in the early and late stage sulfides, respectively. This suggests that the reduced sulfur responsible for the early stage precipitation is bacteriogenic and the late stage sulfur was likely produced by thermochemical sulfate reduction (Tang et al., 2014). The Hg of early stage fluids experienced significant MDF, compared to that of late stage fluids

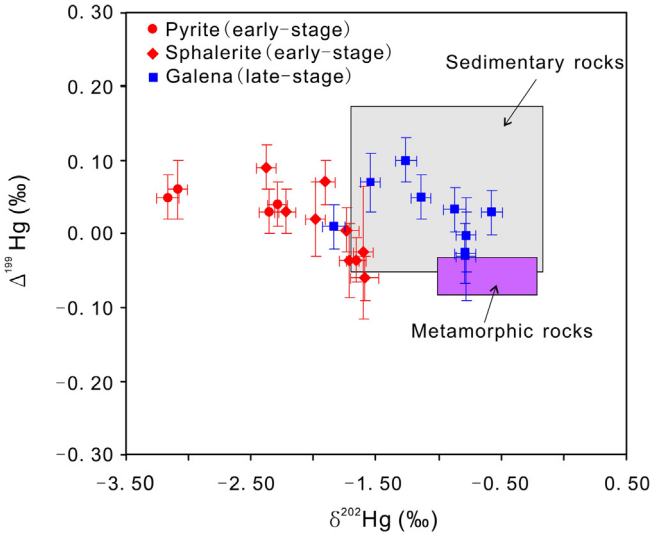


**Fig. 8.** Plot of $\Delta^{199}$Hg vs. $\delta^{202}$Hg values, displaying a comparison of Hg isotopes between the Jinding deposit and lithological reservoirs. The ranges of the sedimentary rocks and metamorphic rocks are defined by the data from Blum et al. (2014) and Smith et al. (2008). The error bars indicate 2σ uncertainties of $\Delta^{199}$Hg and $\delta^{202}$Hg data.

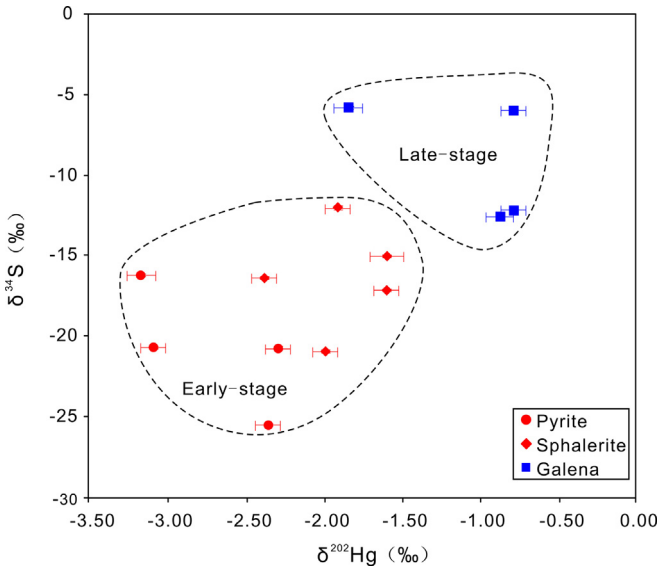


**Fig. 9.** Plot of $\delta^{34}$S vs. $\delta^{202}$Hg values of sulfides from the Jinding deposit. The 2σ uncertainties of $\delta^{34}$S and $\delta^{202}$Hg are indicated, but for $\delta^{34}$S the error bars are covered by the symbols. Note that some samples which are analyzed for Hg isotope compositions lack sulfur isotope data (Table 1) and therefore are not plotted.

that have little fractionation from its sources. These provide a basic framework for a construction of the mineralization history of the Jinding deposit.

During formation, early stage ore fluids, largely composed of formation water (or pore fluids), leached a wealth of metals (e.g., Zn, Pb and Hg) during circulation at depth of the Lanping Basin, and were ultimately driven by the intensive compression associated with collision of the Indian-Asian continents in Cenozoic and ascended along deep-seated faults (Hou et al., 2008). When the fluids moved to low pressure, the aqueous Hg(0) was triggered to volatilize, leading to an isotopically light Hg(0) enrichment in the upper part of the hydrothermal fluid system that was subsequently oxidized to Hg(II) at near-surface environments. As the metalliferous fluids ran into a bacteriogenic $H_2S$ trap at the Jinding dome, sulfides were rapidly precipitated with incorporation of Hg. For late stage mineralization, the meteoric water-dominated fluid might have percolated and dissolved sedimentary evaporite layers to acquire metals (e.g., Gao, 1991). Since the fluid was oxidizing, dissolved Hg existed mainly as Hg(II) that was less fractionated during its transport to the mineralization site. When the fluid carrying metals and $SO_4^{2-}$ flowed through the Jinding dome $SO_4^{2-}$ was thermochemically reduced by hydrocarbons to $H_2S$, which caused Hg precipitation along with Pb and Zn.

## 6. Conclusions

The results of our study show that Hg largely occurs as isomorphic substitution for Zn in sphalerite at the Jinding deposit. Small but significant Hg-MIF is observed in both early and late stage samples without any substantial difference between stages. This indicates that the Hg was likely sourced from sedimentary rocks because of the similar variations of $\Delta^{199}$Hg values to that of sedimentary reservoirs. However, the deposit displays a wide range of $\delta^{202}$Hg values that are enriched in light isotopes in the early stage samples but become heavier in the late stage samples. This implies significant MDF during the transport and/or deposition of Hg in the early stage fluids. The fractionation was likely associated with the boiling of fluids, reduction of Hg(II) to Hg(0), as well as precipitation of Hg sulfides. The Hg of late stage fluids has little

fractionation from its sources. The Hg isotopes in combination with conventional geochemical data would provide more constraints on source of ore-forming materials and fluid evolutions. Although only a preliminary interpretation, with not insignificant uncertainties (e.g., on mechanisms of isotopic fractionation), is presented for the variability of Hg isotopes observed in the Jinding deposit, the potential of Hg isotopes used as a new tracer in study of ore deposits is evident. Moving forward, more studies are required to specifically focus on the Hg isotope compositions of different lithological reservoirs, fractionations associated with Hg transport, redox transformation, and precipitation in hydrothermal fluids, in order to mature the application of Hg to economic geology.

## Acknowledgements

The research is jointly supported by the National Basic Research Program (2015CB452603), Natural Science Foundation (41303014), Institute of Geochemistry, Chinese Academy of Sciences (CAS) (Y5CJ002000 and 201401) and China Scholarship Council (201404910273). David P. Krabbenhoft from the USGS Wisconsin Mercury Research Lab and James P. Hurley from University of Wisconsin-Madison are thanked for providing instrument and lab space. We especially thank Ryan Sharpe from the University of Manitoba for language polishing and two anonymous reviewers for their insightful and constructive comments.

## References

Bai, J.F., Wang, C.H., Na, R.X., 1985. Geological characteristics of the Jinding lead-zinc deposit in Yunnan with a special discussion on its genesis. Miner. Deposits 4, 1–9 (in Chinese with English abstract).
Barnes, H.L., Seward, T.M., 1997. Geothermal Systems and Mercury Deposits. Geochemistry of Hydrothermal Ore Deposits. John Wiley & Sons, New York, pp. 699–736.
Bergquist, B.A., Blum, J.D., 2007. Mass-dependent and -independent fractionation of Hg isotopes by photoreduction in aquatic systems. Science 318, 417–420.
Bergquist, B.A., Blum, J.D., 2009. The odds and evens of mercury isotopes: applications of mass-dependent and mass-independent isotope fractionation. Elements 5, 353–357.
Bessinger, B.A., 2014. Use of stable isotopes to identify sources of mercury in sediments: a review and uncertainty analysis. Environ. Forensics 15, 265–280.
Bingqiu, Z., Jinmao, Z., Lixin, Z., Yaxin, Z., 1986. Mercury, arsenic, antimony, bismuth and boron as geochemical indicators for geothermal areas. J. Geochem. Explor. 25, 379–388.
Biswas, A., Blum, J.D., Bergquist, B.A., Keeler, G.J., Xie, Z.Q., 2008. Natural mercury isotope variation in coal deposits and organic soils. Environ. Sci. Technol. 42, 8303–8309.
Blum, J.D., Bergquist, B.A., 2007. Reporting of variations in the natural isotopic composition of mercury. Anal. Bioanal. Chem. 388, 353–359.
Blum, J.D., Johnson, M.W., Gleason, J.D., Demers, J.D., Landis, M.S., Krupa, S., 2012. Mercury concentration and isotopic composition of epiphytic tree lichens in the Athabasca Oil Sands. In: Percy, K.E. (Ed.), Alberta Oil Sands: Energy. Industry and the Environment, Elsevier, Oxford, UK.
Blum, J.D., Sherman, L.S., Johnson, M.W., 2014. Mercury isotopes in earth and environmental sciences. Annu. Rev. Earth Planet. Sci. 42, 249–269.
Buchachenko, A.L., 2013. Mass-independent isotope effects. J. Phys. Chem. 117, 2231–2238.
Butler, I.B., Archer, C., Vance, D., Oldroyd, A., Rickard, D., 2005. Fe isotope fractionation on FeS formation in ambient aqueous solution. Earth Planet. Sci. Lett. 236, 430–442.
Canil, D., Crockford, P.W., Rossin, R., Telmer, K., 2015. Mercury in some arc crustal rocks and mantle peridotites and relevance to the moderately volatile element budget of the Earth. Chem. Geol. 396, 134–142.
Carignan, J., Estrade, N., Sonke, J.E., Donard, O.F.X., 2009. Odd isotope deficits in atmospheric Hg measured in lichens. Environ. Sci. Technol. 43, 5660–5664.
Chandan, P., Ghosh, S., Bergquist, B.A., 2014. Mercury isotope fractionation during aqueous photoreduction of monomethylmercury in the presence of dissolved organic matter. Environ. Sci. Technol. 49, 259–267.
Chen, J., Hintelmann, H., Feng, X., Dimock, B., 2012. Unusual fractionation of both odd and even mercury isotopes in precipitation from Peterborough, ON. Canada Geochim. Cosmochim. Acta 90, 33–46.
Cook, N.J., Ciobanu, C.L., Pring, A., Skinner, W., Shimizu, M., Danyushevsky, L., Saini-Eidukat, B., Melcher, F., 2009. Trace and minor elements in sphalerite: a LA-ICPMS study. Geochim. Cosmochim. Acta 73, 4761–4791.
Cooke, C.A., Hintelmann, H., Ague, J.J., Burger, R., Biester, H., Sachs, J.P., 2013. Use and legacy of mercury in the andes. Environ. Sci. Technol. 47, 4181–4188.
Donovan, P.M., Blum, J.D., Yee, D., Gehrke, G.E., Singer, M.B., 2013. An isotopic record of mercury in San Francisco Bay sediment. Chem. Geol. 349–350, 87–98.
Ehrlich, S., Butler, I., Halicz, L., Rickard, D., Oldroyd, A., Matthews, A., 2004. Experimental study of the copper isotope fractionation between aqueous Cu(II) and covellite, CuS. Chem. Geol. 209, 259–269.
Estrade, N., Carignan, J., Sonke, J.E., Donard, O.F.X., 2009. Mercury isotope fractionation during liquid–vapor evaporation experiments. Geochim. Cosmochim. Acta 73, 2693–2711.
Estrade, N., Carignan, J., Donard, O.F.X., 2010. Isotope tracing of atmospheric mercury sources in an urban area of northeastern France. Environ. Sci. Technol. 44, 6062–6067.
Fedikow, M.A.F., Amor, S.D., 1990. Evaluation of a mercury-vapour detection system in base- and precious-metal exploration, northern Manitoba. J. Geochem. Explor. 38, 351–374.
Fein, J.B., Williams-Jones, A.E., 1997. The role of mercury-organic interactions in the hydrothermal transport of mercury. Econ. Geol. 92, 20–28.
Feng, X., Li, G., Qiu, G., 2004. A preliminary study on mercury contamination to the environment from artisanal zinc smelting using indigenous methods in Hezhang county, Guizhou, China—Part 1: mercury emission from zinc smelting and its influences on the surface waters. Atmos. Environ. 38, 6223–6230.
Fitzgerald, W.F., Lamborg, C.H., 2003. Geochemistry of mercury in the environment. In: Holland, H.D., Turekian, K.K. (Eds.), Environmental Geochemistry. Elsevier, Oxford, UK, pp. 107–148. Treatise Geochem. 9.
Fitzgerald, W.F., Engstrom, D.R., Lamborg, C.H., Tseng, C.M., Balcom, P.H., Hammerschmidt, C.R., 2005. Modern and historic atmospheric mercury fluxes in northern alaska: global sources and arctic depletion. Environ. Sci. Technol. 39, 557–568.
Foucher, D., Hintelmann, H., 2006. High-precision measurement of mercury isotope ratios in sediments using cold-vapor generation multi-collector inductively coupled plasma mass spectrometry. Anal. Bioanal. Chem. 384, 1470–1478.
Gantner, N., Hintelmann, H., Zheng, W., Muir, D.C., 2009. Variations in stable isotope fractionation of Hg in food webs of arctic lakes. Environ. Sci. Technol. 43, 9148–9154.
Gao, G.L., 1991. Formation age and involved problems on anhydrite ore in Jinding lead-zinc ore area. Yunnan Geol. 10, 191–206 (in Chinese with English abstract).
Gao, L., Wang, A.J., Liu, J.L., Xiu, Q.Y., Cao, D.H., Zhai, Y.F., 2005. New progress in study of superlarge Jinding Pb-Zn deposit: discovery of intrusive breccia and its geological implications. Miner. Deposits 24, 457–461 (in Chinese with English abstract).
Gehrke, G.E., Blum, J.D., Meyers, P.A., 2009. The geochemical behavior and isotopic composition of Hg in amid-Pleistocene western Mediterranean sapropel. Geochim. Cosmochim. Acta 73, 1651–1665.
Gehrke, G.E., Blum, J.D., Marvin-DiPasquale, M., 2011. Sources of mercury to San Francisco Bay surface sediment as revealed by mercury stable isotopes. Geochim. Cosmochim. Acta 75, 691–705.
Ghosh, S., Schauble, E.A., Lacrampe Couloume, G., Blum, J.D., Bergquist, B.A., 2013. Estimation of nuclear volume dependent fractionation of mercury isotopes in equilibrium liquid–vapor evaporation experiments. Chem. Geol. 336, 5–12.
Grammatikopoulos, T.A., Valeyev, O., Roth, T., 2006. Compositional variation in Hg-bearing sphalerite from the polymetallic Eskay Creek deposit, British Columbia, Canada. Chemie der Erde – Geochemi 66, 307–314.
Gratz, L.E., Keeler, G.J., Blum, J.D., Sherman, L.S., 2010. Isotopic composition and fractionation of mercury in great lakes precipitation and ambient Air. Environ. Sci. Technol. 44, 7764–7770.
Hintelmann, H., 2012. Use of stable isotopes in mercury research. In: Bank, A.S. (Ed.), Mercury Environ.: Pattern Process. University of California Press, Los Angeles, pp. 55–71.
Holland, H.D., 1972. Granites, solutions, and base metal deposits. Econ. Geol. 67, 281–301.
Hou, Z.Q., Song, Y.C., Li, Z., Wang, Z.L., Yang, Z.M., Yang, Z.S., Liu, Y.C., Tian, S.H., He, L. Q., Chen, K.X., Wang, F.C., Zhao, C.X., Xue, W.Z., Lu, H.F., 2008. Thrust-controlled, sediment-hosted Pb-Zn-Ag-Cu deposits in eastern and northern margins of Tibetan orogenic belt: geological features and tectonic model. Miner. Deposits 27, 123–144 (in Chinese with English abstract).
Hu, R.Z., Turner, G., Burnard, P.G., Zhong, H., Ye, Z.J., Bi, X.W., 1998. Helium and argon isotopic geochemistry of Jinding superlarge Pb-Zn deposit. Sci. China (Series D) 41, 442–448.
Hu, G.Y., Li, Y.H., Zeng, P.S., 2013. The role of halosalt in mineralization of the Jinding Pb-Zn deposit: evidence from sulfur and strontium isotopic compositions. Acta Geol. Sinica 11, 1695–1702 (in Chinese with English abstract).
Kyle, J.R., Li, N., 2002. Jinding: a jiant tertiary sandstone-hosted Pb-Zn deposit, Yunnan, China. SEG Newsletter 50, 9–16.
Laffont, L., Sonke, J.E., Maurice, L., Hintelmann, H., Pouilly, M., Sánchez Bacarreza, Y., 2009. Anomalous mercury isotopic compositions of fish and human hair in the bolivian amazon. Environ. Sci. Technol. 43, 8985–8990.
Leach, D.L., Song, Y., Hou, Z., 2016. The world-class Jinding Zn-Pb deposit: ore formation in an evaporite dome, Lanping Basin, Yunnan, China. Miner. Deposita, 668–673. online.
Lefticariu, L., Blum, J.D., Gleason, J.D., 2011. Mercury isotopic evidence for multiple mercury sources in coal from the illinois basin. Environ. Sci. Technol. 45, 1724–1729.
Li, N., 1998. Depositional Controls and Genesis of the Jinding Sandstonehosted Zn-Pb Deposit, Yunnan Province, Southwest China Ph.D. Thesis. University of Texas, Austin, pp. 1-100.

Li, X.Z., Liu, W.J., Wang, Y.Z., Zhu, Q.W., Du, D.X., Shen, G.F., Liu, C.J., Que, M.Y., Yang, S.H., Li, D.M., Feng, Q.L., 1999. The Tectonic Evolution and Metallogenesis in the Tethys of the Nujiang-Lancangjiang-Jinshajiang Area, Southwestern China. Geological Publishing House, Beijing.
Li, Z.G., Feng, X.B., He, T.R., 2005. Determination of total mercury in soil and sediment by aqua regia digestion in the water bath coupled with cold vapour atom fluorescence spectrometry. Bull. China Soc. Mineral Petrol. Geochem. 24, 140–143 (in Chinese).
Li, Y.L., Wang, C.S., Yi, H.S., Liu, Z.F., Li, Y., 2006. Cenozoic thrust system and uplifting of the Tanggula Mountain, Northern Tibet. Acta Geol. Sinica 80, 1118–1131 (in Chinese with English abstract).
Liu, Y.J., Cao, L.M., Li, Z.L., 1984. Geochemistry of Elements. Science Publishing House, Beijing, pp. 548 (in Chinese).
Liu, Z.Q., Li, X.Z., Ye, Q.T., Luo, J.N., Shen, G.F., 1993. Division of Tectono-Magmatic Zones and the Distribution of Deposits in the Sanjiang Area. Geological Publishing House, Beijing (in Chinese with English abstract).
Luo, J.L., Yang, Y.H., Zhao, Z., Chen, J.S., Yang, J.Z., 1994. Evolution of the Tethys in Western Yunnan and Mineralization for Main Metal Deposits. Geological Publishing House, Beijing, pp. 157-215 (in Chinese).
Mo, X.X., Lu, F.X., Shen, S.Y., Zhu, Q.W., Hou, Z.Q., 1993. Volcanism and Metallogeny in the Sanjiang Tethys. Geological Publishing House, Beijing (in Chinese with English abstract).
Mu, C.L., Wang, J., Yu, Q., Zhang, L.S., 1999. The evolution of the sedimentary basin in Lanping area during Mesozoic-Cenozoic. Miner. Petrol. 19, 30–36 (in Chinese with English abstract).
Nelson, C.E., 1990. Comparative geochemistry of jasperoids from Carlin-type gold deposits of the western United States. J. Geochem. Explor. 36, 171–195.
Pan, G.T., Xu, Q., Hou, Z.Q., Wang, L.Q., Du, D.X., Mo, X.X., Li, D.M., Wang, M.J., Jiang, X.S., Hu, Y.Z., 2003. The Ore-Forming System of the Orogenic Processing in the Western "Sangjiang" Ploy-Arc and the Resources Estimate. Geological Publishing House, Beijing.
Pirrone, N., Cinnirella, C., Feng, X., Finkelman, R.B., Friedli, H.R., Leaner, J., Mason, R., Mukherjee, A.B., Stracher, G.B., Streets, D.G., Telmer, K., 2010. Global mercury emissions to the atmosphere from anthropogenic and natural sources. Atmos. Chem. Phys. 10, 5951–5964.
Qin, G.J., Zhu, S.Q., 1991. The ore-forming model of the Jinding lead-zinc deposit and prediction. Yunnan Geol. 10, 145–190 (in Chinese with English abstract).
Saulas, D., 1985. Etude minéraloque et géologique desgites Cantabriques à Ba-Zn-Pb-(Cu)-(Hg) en limite socle-couverture (région de Cabezon de la Sal). Université d'Orleans, France, pp. 257.
Schauble, E.A., 2007. Role of nuclear volume in driving equilibrium stable isotope fractionation of mercury, thallium, and other very heavy elements. Geochim. Cosmochim. Acta 71, 2170–2189.
Schwartz, M.O., 1997. Mercury in zinc deposits: economic geology of a polluting element. Int. Geol. Rev. 39, 905–923.
Senn, D.B., Chesney, E.J., Blum, J.D., Bank, M.S., Maage, A., Shine, J.P., 2010. Stable isotope (N, C, Hg) study of methylmercury sources and trophic transfer in the northern gulf of Mexico. Environ. Sci. Technol. 44, 1630–1637.
Sherman, L.S., Blum, J.D., Nordstrom, D.K., McCleskey, R.B., Barkay, T., Vetriani, C., 2009. Mercury isotopic composition of hydrothermal systems in the Yellowstone Plateau volcanic field and Guaymas Basin sea-floor rift. Earth Planet. Sci. Lett. 279, 86–96.
Sherman, L.S., Blum, J.D., Johnson, K.P., Keeler, G.J., Barres, J.A., Douglas, T.A., 2010. Mass-independent fractionation of mercury isotopes in Arctic snow driven by sunlight. Nat. Geosci. 3, 173–177.
Sherman, L.S., Blum, J.D., Keeler, G.J., Demers, J.D., Dvonch, J.T., 2012. Investigation of local mercury deposition from a coal-fired power plant using mercury isotopes. Environ. Sci. Technol. 46, 382–390.
Shi, J.X., Yi, F.H., Wen, Q.D., 1983. The rock-ore characteristics and mineralization of Jinding lead-zinc deposit, Lanping. Yunnan Geol. 2, 179–195 (in Chinese with English abstract).
Smith, R.H., Martell, A.E., 1989. Critical stability constants 6: second suppl., Plenum, New York.
Smith, C.N., Kesler, S.E., Klaue, B., Blum, J.D., 2005. Mercury isotope fractionation in fossil hydrothermal systems. Geology 33, 825–828.
Smith, C.N., Kesler, S.E., Blum, J.D., Rytuba, J.J., 2008. Isotope geochemistry of mercury in source rocks, mineral deposits and spring deposits of the California Coast Ranges. USA. Earth Planet. Sci. Lett. 269, 399–407.
Smith, R.S., Wiederhold, J.G., Jew, A.D., Brown Jr, G.E., Bourdon, B., Kretzschmar, R., 2014. Small-scale studies of roasted ore waste reveal extreme ranges of stable mercury isotope signatures. Geochim. Cosmochim. Acta 137, 1–17.
Smith, R.S., Wiederhold, J.G., Kretzschmar, R., 2015. Mercury isotope fractionation during precipitation of metacinnabar (β-HgS) and montroydite (HgO). Environ. Sci. Technol. 49, 4325–4334.
Song, Y.C., Hou, Z.Q., Yang, T.N., Zhang, H.R., Yang, Z.S., Tian, S.H., Liu, Y.C., Wang, X.H., Liu, Y.X., Xue, C.D., Wang, G.H., Li, Z., 2011. Sediment-hosted Himalayan base metal deposits in Sanjiang region: characteristics and genetic types. Acta Peteologica et Mineralogica 30, 355–380 (in Chinese with English abstract).
Sonke, J.E., 2011. A global model of mass independent mercury stable isotope fractionation. Geochim. Cosmochim. Acta 75, 4577–4590.
Sonke, J.E., Blum, J.D., 2013. Advances in mercury stable isotope biogeochemistry Preface. Chem. Geol. 336, 1–4.
Sonke, J.E., Schäfer, J., Chmeleff, J., Audry, S., Blanc, G., Dupré, B., 2010. Sedimentary mercury stable isotope records of atmospheric and riverine pollution from two major European heavy metal refineries. Chem. Geol. 279, 90–100.
Spurlin, M.S., Yin, A., Horton, B.K., Zhou, J.Y., Wang, J.H., 2005. Structural evolution of the Yushu-Nangqian region and its relationship to syncollisional igneous activity, eastcentral Tibet. GSA Bull. 117, 1293–1317.
Spycher, N., Reed, M.H., 1989. Evolution of a Broadlands-type epithermal fluid along altermative P-T path: implications for the transport and deposition of base, precious and volatile metals. Econ. Geol. 84, 328–359.
Stetson, S.J., Gray, J.E., Wanty, R.B., Macalady, D.L., 2009. Isotopic variability of mercury in ore, mine-waste calcine, and leachates of mine-waste calcine from areas mined for mercury. Environ. Sci. Technol. 43, 7331–7336.
Sun, R., Sonke, J.E., Heimbuerger, L.E., Belkin, H.E., Liu, G., Shome, D., Cukrowska, E., Liousse, C., Pokrovsky, O.S., Streets, D.G., 2014. Mercury stable isotope signatures of world coal deposits and historical coal combustion emissions. Environ. Sci. Technol. 48, 7660–7668.
Tang, Y., Bi, X., He, L., Wu, L., Feng, C., Zou, Z., Tao, Y., Hu, R., 2011. Geochemical characteristics of trace elements, fluid inclusions and carbon-oxygen isotopes of calcites in the Jinding Zn-Pb deposit, Lanping, China. Acta Petrologica Sinica 27, 2635–2645.
Tang, Y.Y., Bi, X.W., Wu, L.Y., Zou, Z.C., He, L.P., 2013. Carbon, oxygen, strontium and lead isotopic geochemistry in the Jinding super-large Zn-Pb deposit, Yunnan Province. Geochemica 42, 467–480 (In Chinese with English abstract).
Tang, Y., Bi, X., Fayek, M., Hu, R., Wu, L., Zou, Z., Feng, C., Wang, X., 2014. Microscale sulfur isotopic compositions of sulfide minerals from the Jinding Zn–Pb deposit, Yunnan Province, Southwest China. Gond. Res. 26, 594–607.
Third Geological Team, 1984. The exploration report of the Jinding Zn-Pb deposit in Lanping County, Yunnan Province. Yunnan Bureau of Geology and Mineral Resources Open-file Report.
Tissot, B.P., Welte, D.H., 1984. Petroleum Formation and Occurrence. Springer, Berlin.
Vaughan, D.J., Rosso, K.M., 2006. Chemical bonding in sulfide minerals. in Vaughan, D.J. (Ed), Sulfide Mineralogy and Geochemistry. Rev. Mineral. Geochem. 61, pp. 231–264.
Veeramani, H., Eagling, J., Jamieson-Hanes, J.H., Kong, L.Y., Ptacek, C.J., Blowes, D.W., 2015. Zinc isotope fractionation as an indicator of geochemical attenuation processes. Environ. Sci. Technol. Lett. 2, 314–319.
Wang, E., Burchfiel, B.C., 1997. Interpretation of cenozoic tectonics in the right-lateral accommodation zone between the ailao shan shear zone and the eastern himalayan syntaxis. Int. Geol. Rev. 39, 191–219.
Wang, J.B., Li, C.Y., 1991. REE geochemistry of the Jinding super-large Pb-Zn deposit. Geochimica 20, 359–365 (in Chinese with English abstract).
Wang, A., Cao, D.H., Gao, L., Wang, G.S., Guan, Y., Xiu, Q.Y., Liu, J.L., 2009. A Probe into the genesis of jinding super-large lead-zinc ore deposit. Acta Geol. Sinica 83, 43–54 (in Chinese with English abstract).
Wen, C.Q., Cai, J.M., Liu, W.Z., Qin, G.J., Cheng, S.F., 1995. Geochemical characteristics of fluid inclusions in the Jinding lead-zinc deposit, Yunnan, China. J. Mineral. Petrol. 15, 78–84 (in Chinese with English abstract).
Wiederhold, J.G., 2015. Metal stable isotope signatures as tracers in environmental geochemistry. Environ. Sci. Technol. 49, 2606–2624.
Wiederhold, J.G., Cramer, C.J., Daniel, K., Infante, I., Bourdon, B., Kretzschmar, R., 2010. Equilibrium mercury isotope fractionation between dissolved Hg(II) species and thiol-bound Hg. Environ. Sci. Technol. 44, 4191–4197.
Wiederhold, J.G., Smith, R.S., Siebner, H., Jew, A.D., Brown, G.E., Bourdon, B., 2013. Mercury isotope signatures as tracers for Hg cycling at the New Idria Hg mine. Environ. Sci. Technol. 47, 6137–6145.
Xiu, Q.Y., Gao, L., Wang, A.J., Liu, J.L., Cao, D.H., Fan, S.J., Zhai, Y.F., 2006. Discovery of Plaeoproterozoic zircon SHRIMP age from Jinding deposit and its geological implications. Acta Petrologica Sinica 22, 1040–1048 (in Chinese with English abstract).
Xue, C.J., Chen, Y.C., Wang, D.H., Yang, J.M., Yang, W.G., 2003. Geology and isotopic composition of helium, neon, xenon and metallogenic age of the Jinding and Baiyangping ore deposits, northwest Yunnan, China. Sci. China (Series D) 46, 789–800.
Xue, C.J., Zeng, R., Liu, S.W., Chi, G.X., Qing, H.R., Chen, Y.C., Yang, J.M., Wang, D.H., 2007a. Geologic, fluid inclusion and isotopic characteristics of the Jinding Zn-Pb deposit, western Yunnan, South China: a review. Ore Geol. Rev. 31, 337–359.
Xue, C.J., Chi, G.X., Chen, Y.C., Zeng, R., Gao, Y.B., Qing, H.R., 2007b. Fluid dynamic processes of large-scale mineralization in the Lanping Basin, Yunnan, SW-China: evidence from fluid inclusions and basin fluid modeling. Earth Sci. Front. 14, 147–157 (in Chinese with English abstract).
Yin, A., Harrison, T.M., 2000. Geologic evolution of the Himalayan-Tibetan orogen. Annu. Rev. Earth Planet. Sci. 28, 211–280.
Yin, R., Feng, X., Li, Z., Zhang, Q., Bi, X., Li, G., Liu, J., Zhu, J., Wang, J., 2012. Metallogeny and environmental impact of Hg in Zn deposits in China. Appl. Geochem. 27, 151–160.
Yin, R., Feng, X., Wang, J., Li, P., Liu, J., Zhang, Y., Chen, J., Zheng, L., Hu, T., 2013. Mercury speciation and mercury isotope fractionation during ore roasting process and their implication to source identification of downstream sediment in the Wanshan mercury mining area, SW China. Chem. Geol. 336, 72–79.
Yin, R., Feng, X., Li, X., Yu, B., Du, B., 2014. Trends and advances in mercury stable isotopes as a geochemical tracer. Trends Environ. Anal. Chem. 2, 1–10.
Yin, R., Feng, X., Hurley, J.P., Krabbenhoft, D.P., Lepak, R.F., Hu, R., Zhang, Q., Li, Z., Bi, X., 2016a. Mercury isotopes as proxies to identify sources and environmental impacts of mercury in sphalerites. Sci. Rep. 6, 1–8.
Yin, R., Krabbenhoft, D.P., Bergquist, B.A., Zheng, W., Lepak, R.F., Hurley, J.P., 2016b. Effects of mercury and thallium concentrations on high precision determination of mercury isotopic composition by Neptune Plus multiple collector inductively coupled plasma mass spectrometry. J. Anal. At. Spectrom. 31, 2060–2068.

You, Y., Li, X., 1990. Research and application of soil-gas mercury surveys for locating deep uranium orebodies. J. Geochem. Explor. 38, 133–143.
Zambardi, T., Sonke, J.E., Toutain, J.P., Sortino, F., Shinohara, H., 2009. Mercury emissions and stable isotopic compositions at Vulcano Island (Italy). Earth Planet. Sci. Lett. 277, 236–243.
Zeng, R., 2007. The large scale fluid ore-forming process in the Lanping basin-taking the Jinding and Baiyangping deposits as the examples (Ph.D. Thesis). Chang'an University, Xi'an, pp. 1–82 (in Chinese with English abstract).
Zhang, H., Yin, R.S., Feng, X.B., Sommar, J., Anderson, C.W.N., Sapkota, A., Fu, X.W., Larssen, T., 2013. Atmospheric mercury inputs in montane soils increase with elevation: evidence from mercury isotope signatures. Sci. Rep. 3, 1–8.
Zhao, H., 2006. Study on the Characteristics and Metallogenic Conditions of Copper-polymetallic Deposits in Middle-northern Lanping Basin, Western Yunnan (Ph. D. Thesis). China University of Geosciences, Beijing, pp. 1-109 (in Chinese with English abstract).
Zheng, W., Hintelmann, H., 2009. Mercury isotope fractionation during photoreduction in natural water is controlled by its Hg/DOC ratio. Geochim. Cosmochim. Acta 73, 6704–6715.
Zheng, W., Hintelmann, H., 2010. Nuclear field shift effect in isotope fractionation of mercury during abiotic reduction in the absence of light. J. Phys. Chem. A 114, 4238–4245.
Zheng, W., Foucher, D., Hintelmann, H., 2007. Mercury isotope fractionation during volatilization of Hg(0) from solution into the gas phase. J. Anal. At. Spectrom. 22, 1097–1104.
Zhong, K.H., Tang, J.X., Liu, Z.C., Kou, L.L., Dong, S.Y., Li, Z.J., Zhou, H.W., 2006. Mesozoic-Cenozoic intracontinental rifting of Changdu-Simao tectonic zone in east margin of Qinghai-Tibet, SW China. Acta Geol. Sinica 9, 1296–1311 (in Chinese with English abstract).